

Iodosulfuron degradation by TiO₂ photocatalysis: Kinetic and reactional pathway investigations

Mohamad Sleiman^{*}, Pierre Conchon, Corinne Ferronato, Jean-Marc Chovelon

*Laboratoire d'Application de la Chimie à l'Environnement, UMR CNRS 5634, Université Claude Bernard Lyon 1,
43 Bd du 11 Novembre 1918, 69622 Villeurbanne Cedex, France*

Received 7 July 2006; received in revised form 10 September 2006; accepted 17 September 2006
Available online 30 October 2006

Abstract

The photocatalytic degradation of a sulfonylurea herbicide, iodosulfuron methyl ester (IOME), has been studied in TiO₂ aqueous suspensions under UV irradiation. The influence of various parameters such as initial concentration, TiO₂ concentration and light intensity on the kinetic process was investigated. Disappearance rate of iodosulfuron followed pseudo-first order kinetics. A special attention was devoted to the identification of intermediates, using a new analytical approach which consists of coupling HPLC–DAD (UV), HPLC–ESI–MS and HPLC–¹H NMR techniques after a SPE pre-concentration step. By combining UV, MS and NMR data, up to 20 degradation products were unambiguously identified. Furthermore, ¹H NMR data allowed the differentiation of several positional isomers, in particular those of hydroxylation resulting from the attack of OH radicals on the benzene ring of IOME. Kinetic evolution profiles of main intermediates, end products (NO₃[−], NH₄⁺, SO₄^{2−}) and total organic carbon (TOC) were also examined in detail. From obtained kinetic and analytical results, the presence of privileged sites for the attack of OH radicals was shown and a detailed degradation pathway was proposed.

© 2006 Elsevier B.V. All rights reserved.

Keywords: Photocatalysis; TiO₂; Sulfonylurea; Iodosulfuron; Photocatalytic degradation; Identification; HPLC–MS; HPLC–NMR

1. Introduction

At present, one unresolved problem is the pollution of soils and aquatic systems by chemicals used in agriculture. A recently used herbicide is iodosulfuron-methyl-ester (see Fig. 1), member of sulfonylurea group, which is widely used for control of some annual grasses and broadleaved weeds in several different crops and especially in cereals. Like other sulfonylureas (Sus), IOME is an inhibitor of acetolactate synthase and characterized by a relatively high solubility in water and low chemical and biochemical degradation rates [1]. Furthermore, IOME and its metabolites may persist in soil for several months [2]. These factors could result in a contamination of surface and ground waters, which in turn becomes a potential risk for the environment. As a consequence, it is important to use treatment methods for the removal of this pollutant from water.

Among the remediation methods commonly used, heterogeneous photocatalysis has proved to be one of the most efficient methods for the elimination of environmental pollutants [3–7]. This technique is based upon the use of UV-irradiated semiconductors, usually titanium dioxide (TiO₂) to produce strongly oxidizing species, such as hydroxyl radicals (OH[•]), holes (h⁺), superoxide (O₂^{•−}) and perhydroxy (HOO[•]) which are able to destroy a large variety of toxic organic compounds. Ideally, the end products are carbon dioxide, water, and inorganic ions.

Recent studies have showed that Sus are easily destroyed by photocatalysis using TiO₂ in aqueous suspension [8–11]. The proposed degradation pathways involve several steps: hydroxylations of the aromatic ring, aromatic ring opening, cleavages of the sulfonylurea bridge and mineralization. In the case of Sus containing a triazine ring, incomplete mineralization and formation of cyanuric acid as the final organic product were observed. For characterization of intermediates, HPLC–MS was frequently used due to the poor thermal stability and low volatility of most degradation products. However, unambiguous identification of the unknowns as well as the distinction of

^{*} Corresponding author. Tel.: +33 4 72 43 11 50; fax: +33 4 72 44 84 38.
E-mail address: mohamad.sleiman@univ-lyon1.fr (M. Sleiman).

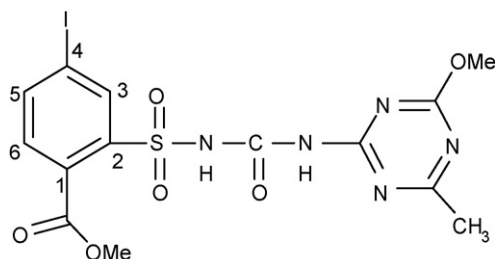


Fig. 1. Chemical structure of iodosulfuron-methyl-ester (IOME).

positional isomers, such as the hydroxylation isomers resulting from the attack of OH radicals on the aromatic ring, remains difficult even if MS/MS or MSⁿ experiments were included [12].

In a work previously reported, a new analytical approach using coupling of HPLC–MS and HPLC–NMR techniques has been developed and applied to identify the intermediates resulting from the photocatalytic degradation of IOME [13]. However, this study was only limited to the characterization of intermediates and no information was given about the kinetic aspects of the process (adsorption, photolysis, degradation rate, etc.) neither on the formation of carboxylic acids, end products, and TOC removal. Furthermore, the proposed degradation pathway was simplified and several reaction steps were not determined. In the present investigation, a completed and detailed study of the IOME degradation is shown. Different topics were studied: (a) IOME disappearance kinetics and the influence of several operational parameters, (b) analysis of intermediates as well as carboxylic acids and their kinetic evolution profiles during the process to give insight into the reaction mechanism and (c) monitoring of mineralization end products and total organic carbon (TOC).

2. Experimental

2.1. Reagents and materials

Iodosulfuron-methyl-ester (IOME) (methyl 4-iodo-2-[[[(4-methoxy-6-methyl-1,3,5-triazin-2-yl) amino] carbonyl] amino]sulfonyl]-benzoate (purity >98%) was provided by Bayer Crop Science (Lyon, France). The photocatalyst used was TiO₂, Degussa P-25, mainly anatase, with a specific BET area of 50 m² g⁻¹ and a mean particle size of 30 nm. Polyvinylidene fluoride (PVDF, i.e., [-(CH₂-CF₂)_n-]) filters (0.45 μm) were purchased from Millipore (Bedford, USA). The following standards were purchased from Aldrich (Steinheim, Germany): cyanuric acid [2,4,6-trihydroxy-1,3,5-triazine] (98%), ammelide [2-amino-4,6-dihydroxy-1,3,5-triazine] (97%) and AMMT [2-amino-4-methoxy-6-methyl-1,3,5-triazine] (97%). Acetonitrile (quality HPLC grade and quality NMR), methanol (HPLC grade) and deuterium oxide (99.9%) were purchased from SDS (Peypin, France). Water was obtained from a Millipore Waters Milli-Q water purification system. *Ortho*-phosphoric acid (85%) and formic acid (MS grade, 99% purity) were from Aldrich. Other reagents were at least of analytical grade.

2.2. Photoreactor and light source

The irradiation experiments were carried out in an open Pyrex glass cell (cut-off at 295 nm, 4.0 cm diameter, 2.3 cm height), containing 25 mL of the aqueous suspension of IOME and TiO₂ powder. The light source was a HPK 125 W Philips mercury lamp with main emission wavelength at 365 nm, cooled with a water circulation. The light intensity was regulated by including calibrated grids between the lamp and the reactor. The light flux entering the irradiation cell was measured by uranylactate actinometry. For all experiments, the cell temperature during irradiation was adjusted to 20 °C, the suspensions were magnetically stirred and the concentration of TiO₂ was optimized at 2.5 g L⁻¹.

2.3. Sample preparation and preconcentration

Stock solutions of IOME (200 mg L⁻¹) were prepared in ultra-pure water buffered with KH₂PO₄/K₂HPO₄ at pH 6.5 and stored at 4 °C in the dark. More diluted samples of IOME (25, 15, 10 and 5 mg L⁻¹) were prepared from the stock solution and further irradiated to study the primary degradation of IOME and the effects of several parameters on the kinetic rate of the process. For identification of degradation products, stock solution was directly used in irradiation experiments without dilution. During the irradiation, aliquots of the aqueous suspension were collected and filtered, at regular time intervals through 0.45 μm PVDF filters to remove TiO₂ particles. In order to detect and identify the maximum number of degradation products, a SPE preconcentration procedure was developed using two types of SPE cartridges from International Sorbent Technology (IST, Cambridge, UK): (a) isolate C₁₈ (500 mg/6 mL), to extract IOME and its “first generation products” and (b) isolate ENV⁺ (200 mg/6 mL), a hydroxylated, highly cross-linked polystyrene–divinylbenzene copolymer (St–DVB) to concentrate more polar products such as triazine derivatives. The best extraction conditions were: conditioning of the sorbents with 6 mL of methanol followed by 6 mL of pure water. The sorbents were not allowed to dry, and subsequently irradiated samples of IOME (200 mg L⁻¹) of 20 mL volume were passed through the cartridges at a rate of ~3 mL min⁻¹ using a Varian vacuum manifold. For ENV⁺ cartridge, the pH of the samples was adjusted between 2.5 and 2.7 using 40% *ortho*-phosphoric acid. The analytes were eluted twice using 1 mL of methanol at a rate of ~1 mL min⁻¹.

2.4. Analytical determinations

2.4.1. HPLC–UV and HPLC–DAD analyses

The primary degradation of IOME was followed by HPLC–UV (VARIAN 9010 model) after injection of 20 μL of irradiated sample (previously filtered) in the following conditions: column Hypersil BDS C₁₈ (5 μm, 125 mm long × 4 mm i.d.); mobile phase, methanol/water (pH set to 2.8 with *ortho*-phosphoric acid) (45:55, v/v); flow rate 1 mL min⁻¹; wavelength, 234 nm.

The evolution of intermediate products was monitored by Shimadzu VP series HPLC system consisting of LC-10AT binary pump, a SPD-M10A DAD and Shimadzu Class-VP software (Version 5.0). A 20 μL of filtered irradiated samples (25 mg L^{-1}) were directly injected. Chromatographic separation was carried out on a $150 \text{ mm} \times 3 \text{ mm}$ i.d., INTERCHIM HDO C_{18} reversed-phase column ($3 \mu\text{m}$, 128 \AA). The mobile phase was a mixture of acetonitrile (A) and water acidified with formic acid at pH 2.8 (B). The flow rate was set to 0.4 mL min^{-1} and a linear gradient was programmed as follow: 0 min, 5% A; 30 min, 70% A; 33 min, 70% A and 35 min, 100% A.

The formation of carboxylic acids was also analyzed by HPLC–DAD using a COREGEL 87-H3 ($9 \mu\text{m}$, $300 \text{ mm} \times 7.8 \text{ mm}$) cation exchange column and H_2SO_4 , $5.5 \times 10^{-3} \text{ mol L}^{-1}$ (pH 2.0) as mobile phase. The detection wavelength was 210 nm, flow rate was 0.6 mL min^{-1} and the injection volume was $100 \mu\text{L}$.

2.4.2. HPLC–MS analysis

The HPLC–MS identification of intermediates was performed on a HP 1100 LC system (Hewlett-Packard GmbH) consisting of quaternary pump, degasser, autosampler, column oven, and DAD UV detector, interfaced with a HP 1100 MSD quadrupole mass spectrometer equipped with an electrospray ionization source. The chromatographic conditions were similar to those used previously for monitoring the evolution of intermediates by HPLC–DAD. In preliminary experiments, an optimization of the ESI interface and ion optics parameters was accomplished in order to maximize the ionization current signal of analytes. For this purpose, a 200 mg L^{-1} IOME irradiated solution was infused (flow rate $20 \mu\text{L min}^{-1}$) into the ESI interface using the syringe pump incorporated into the mass spectrometer. The optimized electrospray parameters were: spray voltage, 4 kV; cone voltage 80 V; drying gas (nitrogen), 12 L min^{-1} ; nebulizer pressure, 55 psi; source temperature $350 \text{ }^\circ\text{C}$. Mass spectra were acquired in both positive and negative ion modes in a mass range of m/z 80–1000.

2.4.3. HPLC– ^1H NMR analysis

Experiments were conducted on an Agilent 1100 series HPLC system coupled to a UV detector and NMR spectrometer (Bruker, DRX 500 MHz) equipped with a ^1H – $\{^{13}\text{C}\}$ inverse flow probe (3 mm internal diameter of measuring cell) with a detection volume of $60 \mu\text{L}$. The chromatographic equipment was controlled by HyStar PP Version 2.3 software (Bruker, Germany). A BPSU interface (BFSU-O, Bruker) was used for combining the chromatographic system with the NMR spectrometer. Stopped-flow NMR spectra were acquired using XWINNMR software (Version 3.5). The chromatographic separation was performed using acetonitrile and ($\text{D}_2\text{O} + \text{H}_3\text{PO}_4$, pH 2.8) as mobile phase. D_2O was used to minimize the intensity of residual water signal in the NMR spectra. In addition, formic acid used in HPLC–MS experiments was replaced by *ortho*-phosphoric acid in order to avoid signals superposition of analytes and formic acid in the aromatic spectral region. Prior to data acquisition, solvent–signal suppression was achieved using

water suppression enhanced through T_1 effects (WET) solvent suppression and GARP ^{13}C decoupling during WET dephasing and acquisition to suppress ^{13}C satellites of acetonitrile [14]. Depending on the concentration of the analyte in the sample, the total number of scans varied between 64 and 256. Data were multiplied with an exponential function f2 ($\text{LB} = 0.3 \text{ Hz}$) prior to Fourier transformation. ^1H NMR chemical shift values were referenced to methanol which was set to 3.20 ppm.

2.4.4. IC analysis

The formation of inorganic ions was monitored by ion chromatography (IC), using a Dionex DX-120 ion-chromatograph equipped with a Dionex AS 40 autosampler, a conductivity detector and an IonPac AS14A ($4 \times 250 \text{ mm}$) anion exchange column. The eluent was $\text{Na}_2\text{CO}_3/\text{NaHCO}_3$ (8/1 mM). Ammonium ion analysis was performed using the same apparatus, except for column (CS12A, $4 \times 250 \text{ mm}$) and eluent, H_2SO_4 20 mM. All elutions have been carried out at flow rate of 1 mL min^{-1} .

2.4.5. TOC measurements

Total organic carbon (TOC) determinations were carried out using a TOC analyzer Bioritech Model (standard method EPA 415.1) on the filtered irradiated samples of IOME (25 mg L^{-1}).

3. Results and discussions

3.1. Adsorption in the dark and direct photolysis

In order to study the adsorption of IOME and to compare the direct photolysis with photocatalytic activity of TiO_2 , experiments with and without the addition of TiO_2 were carried out. Fig. 2 illustrates the time course of the concentration of IOME ($C_0 = 50 \mu\text{mol L}^{-1}$ equivalent approximately to 25 mg L^{-1}) under three different experimental conditions: (1) in the dark in presence of TiO_2 ; (2) UV irradiation in absence of TiO_2 ; (3) UV irradiation in presence of TiO_2 . As can be seen, the adsorption equilibrium was rapidly reached within 20 min (curve A) and only 5% of IOME ($Q_{\text{ads}} \sim 2.5 \mu\text{mol L}^{-1}$) was adsorbed after 120 min on TiO_2 surface corresponding to a surface coverage of

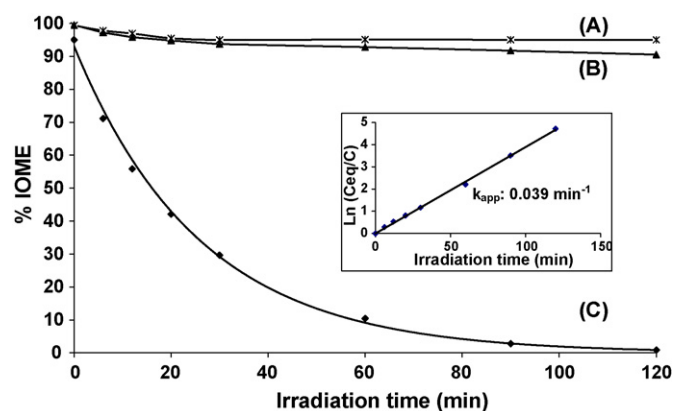


Fig. 2. Adsorption (A), direct photolysis (B) and photocatalytic degradation (C) of IOME ($50 \mu\text{mol L}^{-1}$). The inset shows the linear transform of the integrated first-order kinetics.

less than 0.1 molecule/nm². This represents a low adsorbed organic molecule. Irradiation of IOME in absence of TiO₂ showed no significant photodegradation. After 120 min of irradiation, direct photolysis contributed less than 10% to the degradation process (Fig. 2, curve B) indicating that the photochemical process are scarcely responsible for the observed fast transformation when the solution was irradiated in the presence of TiO₂ (Fig. 2, curve C).

3.2. Kinetic of iodosulfuron disappearance

The kinetic of photocatalytic disappearance of IOME is shown in Fig. 2 (curve C). It can be observed that total disappearance of IOME was achieved quite fast in around 100 min for 2.5 g L⁻¹ TiO₂ concentration and 4 × 10¹⁵ photon s⁻¹ cm⁻² light flux. The quasi-exponential decay observed during irradiation along with the linear plot of ln C_{eq}/C_t versus time (Fig. 2, inset) indicate that, in our experimental conditions, IOME degradation follows a pseudo-first order kinetic with a constant rate of 0.039 ± 0.002 min⁻¹. However, a previous work showed that the first-order rate constant did not remain constant when varying the initial concentration of Sus herbicides, even if the linear form was good and a half order kinetic has been proposed for the degradation of several Sus compounds [8]. Therefore, other experiments were made, under a constant photonic flux (4 × 10¹⁵ photon s⁻¹ cm⁻²), in which the initial concentration of IOME was varied from 2 to 50 μmol L⁻¹ to determine the partial order of the reaction with respect to IOME and also to verify the results obtained by the first method. In these experiments, calculations were done for conversions smaller than 10% in order to avoid the effects of intermediates on the kinetic. Results showed a good linear correlation (R² = 0.993) between the initial rate (r₀) and initial concentration (C_{eq}), which confirms that photocatalytic degradation of IOME followed an apparent first-order kinetic law (r = k_{app}C_{eq}). Although this behavior could be in agreement with a generally observed Langmuir–Hinshelwood (LH) kinetic model (Eq. (1)) when the substrate concentration is low enough and no catalyst saturation occurs, the present kinetic data are not sufficient to conclude that such a mechanism is the most suitable one to describe the photocatalytic process of IOME:

$$r = -\frac{dC}{dt} = k_{LH}\theta = k_{LH} \frac{K_{LH}C_{eq}}{1 + K_{LH}C_{eq}} \quad (1)$$

3.2.1. Effect of TiO₂ concentration

The effect of photocatalyst concentration on the disappearance kinetics of IOME has been investigated employing different TiO₂ concentrations ranging from 0 to 5 g L⁻¹. The first order constant k_{app} was measured under a constant photonic flux of 4 × 10¹⁵ photon s⁻¹ cm⁻² with an initial concentration of IOME equal to 50 μmol L⁻¹. As expected, the rate constant k_{app} increased proportionally to TiO₂ concentration until it reached a plateau around 2.5 g L⁻¹, after which IOME conversion remains practically unchanged. At higher-

concentrations, a screening effect of excess particles occurs, thus masking part of the photosensitive surface active sites and consequently hindering light penetration [15,21]. In this study, the optimum concentration at which all the subsequent experiments were conducted is about 2.5 g L⁻¹.

3.2.2. Effect of photonic flux

Experiments have been made using a photonic flux varying from 0.4 to 4.6 × 10¹⁶ photon s⁻¹ cm⁻² and a constant equilibrium concentration of 47.5 μmol L⁻¹ (after adsorption). Fig. 3 represents the influence of the photonic flux on the first order constant rate of IOME. The curve obtained shows that for photonic fluxes below 10¹⁶ photon s⁻¹ cm⁻², k_{app} is directly proportional to the photonic flux, indicating that most of the incident photons are efficiently converted into active species that act in the degradation mechanism. For higher photonic fluxes, the constant rate varies as the square root of the flux. This means that the efficiency of the photocatalytic process is limited above 10¹⁶ photon s⁻¹ cm⁻² due to the electron–hole recombination which becomes predominant.

3.3. Identification of the organic intermediates

3.3.1. HPLC–UV–ESI–MS

In order to characterize all the organic intermediates, a mixture of three solutions of IOME (200 mg L⁻¹) irradiated for 15 min, 1, and 3 h was analyzed by HPLC–UV–MS (ESI). This sample represents as much as possible the different intermediates at their maximum levels of concentrations as observed by HPLC–DAD. After optimization of conditions, up to 20 intermediates were detected and subsequently identified by interpretation of their UV and MS spectra. Table 1 report a summary of the UV and MS data obtained, along with the proposed structures for the detected byproducts. As can be noted, three principal groups of intermediates can be distinguished: the first one corresponds to intermediates 1–8, containing only the triazine ring, the second includes

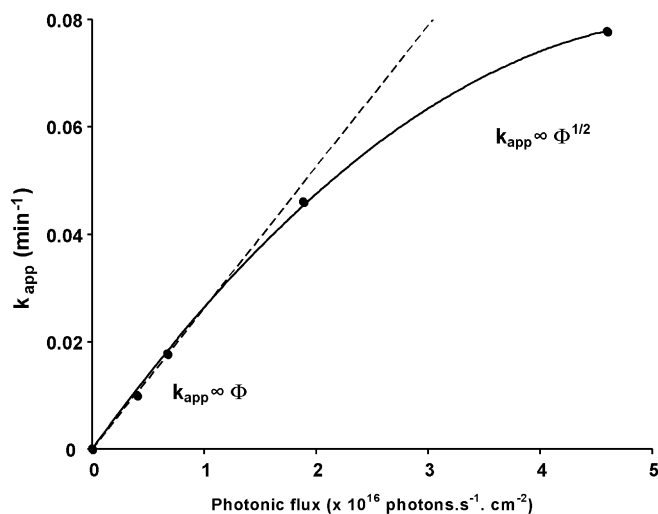


Fig. 3. Influence of the photonic flux on the rate constant of photocatalytic degradation of IOME (50 μmol L⁻¹).

Table 1
UV and MS data for the identification of the intermediate products of iodosulfuron

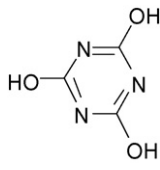
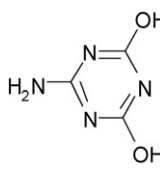
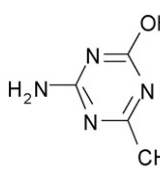
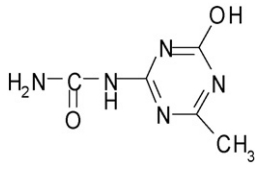
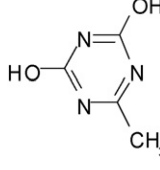
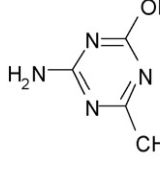
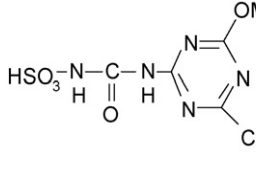
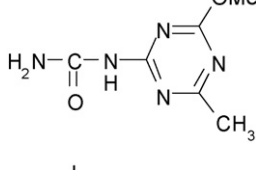
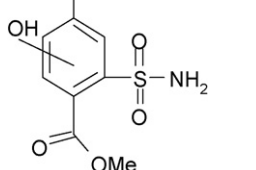
Product	R_t^a (min)	Structure	UV data (λ_{\max} , nm)	MS data ESI, positive/negative mode
1	2.0		198, 224	152 ($M + Na$) ⁺ , 130 ($M + H$) ⁺
2	2.4		200, 226	151 ($M + Na$) ⁺ , 129 ($M + H$) ⁺
3	3.0		195, 225	127 ($M + H$) ⁺
4	3.6		198, 230	192 ($M + Na$) ⁺ , 170 ($M + H$) ⁺ , 127, 168 ($M - H$) ⁻
5	4.8		197, 230	150 ($M + Na$) ⁺ , 128 ($M + H$) ⁺
6	6.4		196, 226	141 ($M + H$) ⁺ , 139 ($M - H$) ⁻
7	7.7		198, 229	264 ($M + H$) ⁺ , 184 ($M - SO_3$) ⁺ , 167, 141, 262 ($M - H$) ⁻
8	10.0		199, 226	206 ($M + Na$) ⁺ , 184 ($M + H$) ⁺ , 167, 141, 182 ($M - H$) ⁻
9	11.1		246, 288	328 ($M + Na$) ⁺ , 306 ($M + H$) ⁺

Table 1 (Continued)

Product	R_f^a (min)	Structure	UV data (λ_{\max} , nm)	MS data ESI, positive/negative mode
10	12.7		240, 290	404 ($M + Na$) ⁺ , 382 ($M + H$) ⁺
11	15.6		232, 286	473 ($M + Na$) ⁺ , 451($M + H$) ⁺ , 127, 153
12	17.0		230, 282	457 ($M + Na$) ⁺ , 435($M + H$) ⁺ , 127, 153
13	18.0		235, 290	502 ($M + Na$) ⁺ , 480 ($M + H$) ⁺ , 127, 153
14	18.7		230, 284	436 ($M + Na$) ⁺ 414 ($M + H$) ⁺ , 167, 141, 412 ($M - H$) ⁻ , 420 ($M + Na$) ⁺
15	19.4			
16	20.1		231, 293	398 ($M + H$) ⁺ , 167, 396 ($M - H$) ⁻
17	20.8		232, 295	516 ($M + Na$) ⁺ , 494 ($M + H$) ⁺ , 127, 153, 492 ($M - H$) ⁻
18	21.3		234, 297	516 ($M + Na$) ⁺ , 494 ($M + H$) ⁺ , 141, 167, 492 ($M - H$) ⁻

Table 1 (Continued)

Product	R_t^a (min)	Structure	UV data (λ_{\max} , nm)	MS data ESI, positive/negative mode
19	23.8		234, 298	546 ($M + Na$) ⁺
20	28.1		524 ($M + H$) ⁺	
21	28.7		141, 167, 522 ($M - H$) ⁻	

^a R_t : retention time.

intermediates **9** and **10** with only a benzene ring in their structures and the third (intermediates **11–21**) is characterized by the presence of both moieties (benzene and triazine rings). More detailed information about the identification of the intermediate products were described in a previous study [13].

3.3.2. HPLC-¹H NMR

Although UV and MS data provided important information on the molecular weight and the presence of certain functional groups, several positional isomers were not discriminated such as products **14**, **15** and **19–21**, resulting from the attack of OH radicals on the benzene ring. Therefore, HPLC-NMR was used to get complementary information and, particularly, to localize the position of hydroxyl group on the benzene ring for these isomers. Since the sensitivity of the NMR detection is low compared to MS, more concentrated sample of IOME (1000 mg L⁻¹) was irradiated for 45 min and, later on, pre-concentrated by SPE. This is the time at which the

concentrations of the isomers **14**, **15** and **19–21** reach their maxima. Fig. 4 depicts relevant regions of the ¹H NMR spectra of IOME and two of its hydroxylation isomers (**19** and **21**), obtained in the stopped-flow mode. As can be seen, the aliphatic regions (2–4 ppm) of spectra B and C, are almost identical to that of IOME (spectrum A), revealing the presence of the methyl moieties (a–c) in both isomers **19** and **21**. On the other hand, the aromatic parts of spectra B and C display only two signals integrated for 1H each, indicating the substitution of one of the three aromatic protons of IOME by a hydroxyl group. Isomer **19** shows two singlets corresponding to H₃ and H₆ whereas isomer **21** exhibits two *ortho*-coupling doublets which are assigned to H₅ and H₆. This finding is corroborated by the chemical shift values of the aromatic protons and by the MS data of products **19** and **21**. Other intermediates were also identified by HPLC-NMR such as byproducts **8**, **14**, **16**, and **17**. The NMR signal assignments for these compounds were summarized elsewhere [13].

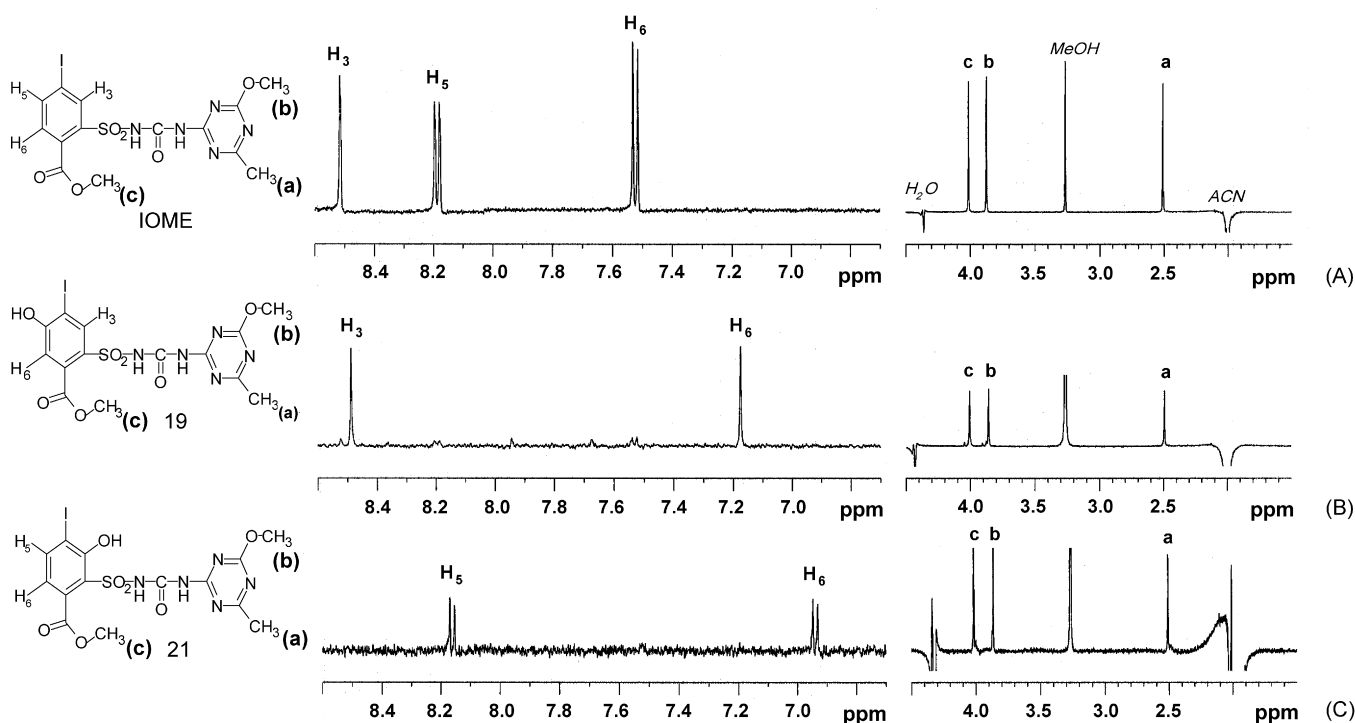


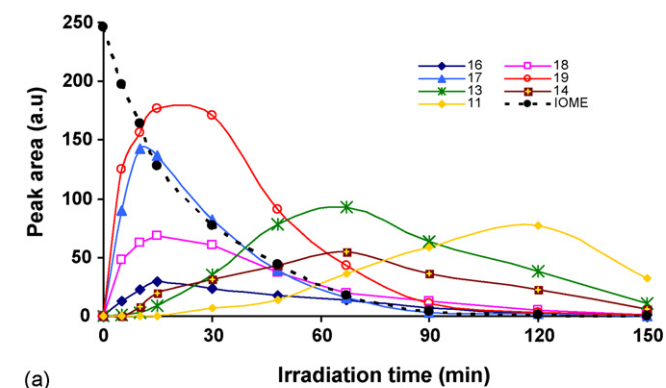
Fig. 4. Relevant regions of ¹H NMR spectra of IOME and its hydroxylation products **19**, **21**, obtained by stopped flow HPLC-NMR analysis of a solution irradiated for 45 min.

3.4. Evolution of intermediates and degradation pathways

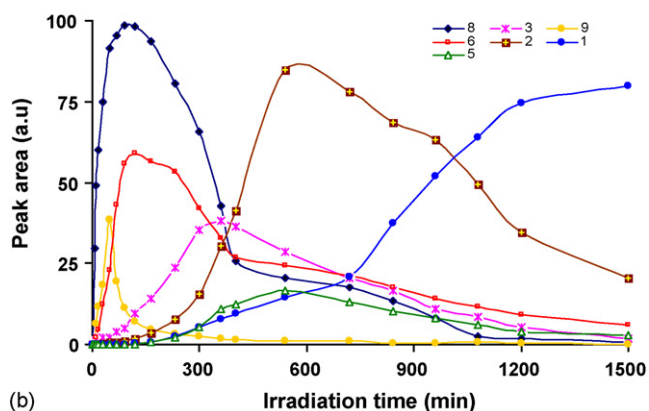
In order to better understand the reaction mechanisms involved in the photocatalytic degradation of IOME, the kinetic evolution of principal intermediates was followed during the irradiation of a solution of IOME (25 mg L^{-1}) under a photonic flux of $4 \times 10^{15} \text{ photon s}^{-1} \text{ cm}^{-2}$.

Based on the identification results, two categories of compounds were distinguished according to the presence or not of the sulfonylurea bridge. The first group (A) gathers the products **11–21** whereas the second (B) includes products **1–10**. Fig. 5-a and -b shows the kinetic behavior of the more abundant intermediates for both groups A and B:

(A) As showed in Fig. 5-a, the first appeared intermediates are the products **16–19** which reach their maximum of concentrations around 15 min then decrease progressively to disappear from solution after 120 min. This finding indicates that the first steps of the degradation seem to be (1) hydroxylation of the benzene ring leading to three hydroxylation products **19–21** (not showed), (2) *O*-demethylation of the methoxy and methyl ester moieties giving arise to products **17** and **18**, respectively, and (3) substitution of the iodide atom by a hydroxyl group which forms the product **16**. By comparing the evolution profiles for these products, it appear that (1) and (2) are the first principal stages of the degradation whereas (3) is much less



(a)



(b)

Fig. 5. (a) Evolution of the intermediates of group (A) during degradation of IOME ($50 \mu\text{mol L}^{-1}$). (b) Evolution of the intermediates of group (B) during degradation of IOME ($50 \mu\text{mol L}^{-1}$).

important because intermediate **16** is formed at very low concentrations while intermediates **17–19** are produced at much higher levels, assuming that the UV response coefficients for these compounds are relatively close. Moreover, considering that the response coefficients for isomers **17–21** in UV and MS detection are similar, one can deduce that:

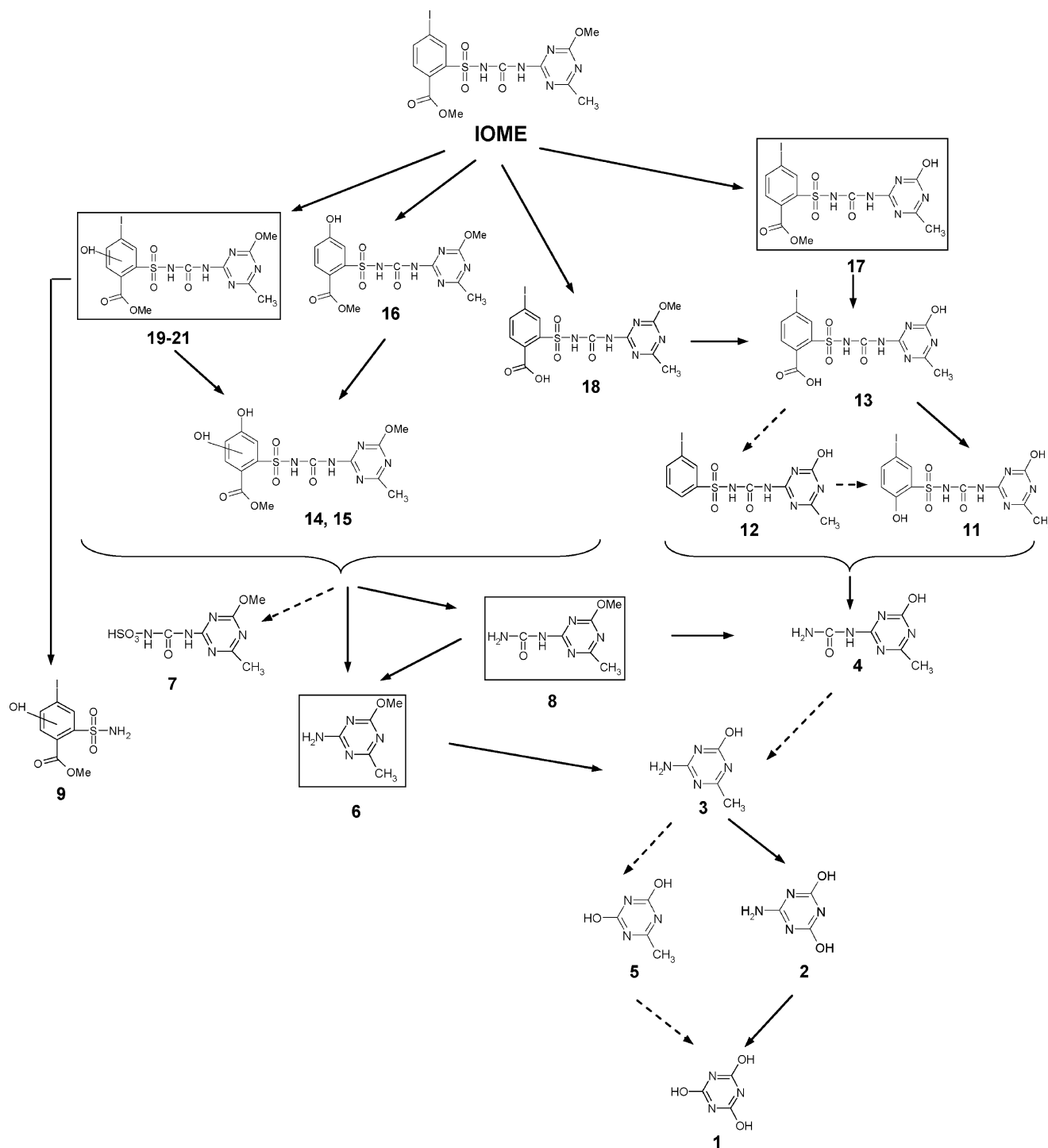
- (i) Isomer **19** is the major hydroxylation product, indicating a regioselective attack for the OH radicals. This result can be explained by the electron density of the benzene carbon sites. In fact, based on the mesomeric and steric hindering effects of the benzene ring substituents ($-\text{COOMe}$, $-\text{SO}_2$ and $-\text{I}$), the site C_5 is more nucleophilic and accessible than the two other sites C_6 and C_3 . As a consequence, the attack of OH radicals, known as strong electrophilic species, takes place preferentially at C_5 and produces compound **19**.
- (ii) Product **17** is more abundant than its isomer **18**, which means that the *O*-demethylation process occurs principally on the methoxy moiety of the triazine ring.

Regarding products **13** and **14**, they appear later on, suggesting that they result from the transformation of the first intermediates (**16–19**). Products **14** and **15** (not represented) can be formed either by a hydroxylation of product **16** or by substitution of iodide atom of the hydroxylation products (**19–21**) by a hydroxyl group whereas the formation of product **13** could be explained by an *O*-demethylation of the methoxy moiety and the methyl ester moiety of products **17** and **18**. As for product **11**, it might result from the decarboxylation of intermediate **13** via photo-kolbe reactions [16]. This hypothesis is supported by the evolution profiles of both products, where compound **11** is not detected before the formation of intermediate **13** and reach its maximum when **13** was completely consumed.

- (B) The second category of intermediates regroups various triazine and benzene derivatives resulting from the cleavages of the sulfonylurea bridge. The evolution of main products belonging to this group is represented on Fig. 5-b. Products **6**, **8** and **9** appear at the first minutes of irradiation and their concentration increases to reach a maximum around 100 min for **9** and 180 min for **6** and **8**. The peak profile of intermediate **9** reveals its fast formation and disappearance kinetics. This can be explained by the high reactivity of OH radicals towards benzene ring, which forms product **9** and proceeds further rapidly by an oxidative opening of the aromatic ring. This behavior was confirmed by the formation of smaller and more oxidized molecules, such as short carboxylic acids (see next paragraph). On the other hand, it is obvious that intermediates **6** and **8** are more stable, since their degradation rates are much slower than that of product **9**. The fast appearance of these products at the first minutes of irradiation suggests their direct formation from IOME via the cleavage of C–N bonds of the sulfonylurea bridge. However, both product concentrations begin to decrease only after 180 min, whereas IOME disappeared from

solution within 120 min. This means that both products can also be produced by the C–N bonds cleavage of sulfonylurea bridge of the intermediates relevant to category (A) such as products **14–16** and **18–21**. Furthermore, the formation of intermediate **6** can be due partially to the cleavage of the urea functional group of product **8**. It should be pointed out that another triazine intermediate (product **7**, not represented in Fig. 5-a) was

also detected during the first minutes of irradiation but at low concentration level compared to intermediates **6** and **8**. The formation of this intermediate can be explained by a C–S bond rupture in the sulfonylurea bridge of IOME, intermediates **14–16** and **18–21**. This observation indicates that the rupture of sulfonylurea bridge occur mainly via the cleavage of C–N bonds whereas the cleavage of C–S bond represent only a minor pathway.



* Dotted arrows represent minor degradation pathways

Fig. 6. Photocatalytic degradation pathway of IOME.

As for product **3**, it is detected only after 60 min of irradiation, thus it is unlikely that it is formed starting from the first generation intermediates (**11–21**). Comparing its evolution profile with that of product **6** lets suppose that it results mainly from an *O*-demethylation of the OCH_3 moiety of intermediate **6**. The formation of other *s*-triazinic compounds at longer irradiation time like products **2** and **5** suggests that the degradation process continues through a series of reactions, including, *O*-demethylation of the methoxy moiety of the triazine and oxidation of methyl and amino groups leading to cyanuric acid (**1**) which cannot undergo further oxidative attacks due to its high resistance to TiO_2 -mediated degradation [17]. In fact, the formation of cyanuric acid as the final organic product observed passes via two parallels routes, the first one is the oxidative attacks of the lateral methyl group to give intermediate **2**, following by a slow oxidation of amino group to nitrate leading to cyanuric acid. The second one is the opposite route, which means that the amino group oxidation of intermediate **3** occurs first and give arise to product **5** which in turn undergoes oxidative attacks of the lateral methyl group yielding cyanuric acid. By regarding the evolution profiles of both Intermediates **2** and **5**, we can conclude that the first route is predominant. This could be explained by the fact that the conversion of amino groups bonded to *s*-triazinic ring is much more difficult than the oxidation of methyl group, by OH radicals [11]. Based on these investigations, a degradation pathway, depicted in Fig. 6, was established showing the formation and transformation of the identified intermediates.

3.5. Identification of aliphatic carboxylic acids

As it has been observed in previous studies [8,11,18], the degradation of both aliphatic and aromatic groups of Sus, leads to the formation of smaller and more oxidized compounds, such as short carboxylic acids. Therefore, irradiated samples of IOME (25 mg L^{-1} equivalent approximately to $50 \mu\text{mol L}^{-1}$) were analyzed by HPLC–DAD to identify the aliphatic carboxylic acids generated during the degradation process. Five major acids were identified (oxalic, formic, acetic, glycolic and glyoxylic) by comparison with commercial standards. Their kinetic evolution during the degradation of IOME is represented in Fig. 7-a. As shown, acetic acid is the major one. Its concentration increases slowly to reach at 120 min a value of $49 \mu\text{mol L}^{-1}$, equivalent to the initial concentration of the IOME, which reveals the transformation of 1 mol of the benzene ring into 1 mol of acetic acid. Formic acid is present during the first 60 min of degradation (maximum of $4 \mu\text{mol L}^{-1}$ after 20 min) then disappears from the solution by transformation into CO_2 . It is again detected after 240 min. Its appearance at the beginning of reaction is undoubtedly due to the oxidation of the $-\text{OCH}_3$ moieties of triazine and benzene ring, whereas its reappearance with 240 min results mainly from the transformation of acetic acid. Oxalic acid appears quickly in solution to reach a maximum of concentration after 50 min of irradiation. Its formation can be explained either by the benzene ring opening or by dimerization of HCO_2 radicals as reported in a previous study [19]. Its disappearance between

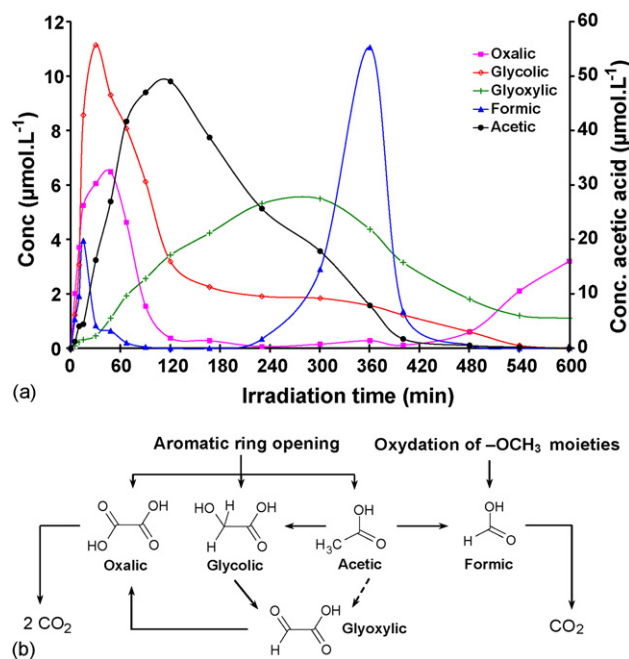


Fig. 7. (a) Formation of carboxylic acids during IOME photocatalytic degradation. (b) Proposed scheme for the formation of carboxylic acids.

150 and 360 min is related to its direct transformation into CO_2 . The oxidation of glycolic acid probably leads to its reappearance beyond 360 min. The opening of the benzene cycle also carries out to the formation of the glycolic acid which reaches its maximum of concentration at 30 min then is transformed partly into glyoxylic acid. A tentative mechanism for the formation of carboxylic acids inferred from these data is showed in Fig. 7-b.

3.6. Evolution of mineralization

Complete mineralization is the ultimate step in water treatment process of organic molecules. It is thus important to follow not only the disappearance of the initial pollutant but also its mineralization into CO_2 and inorganic ions. Looking at the formula for IOME, one can expect the formation of NO_3^- ,

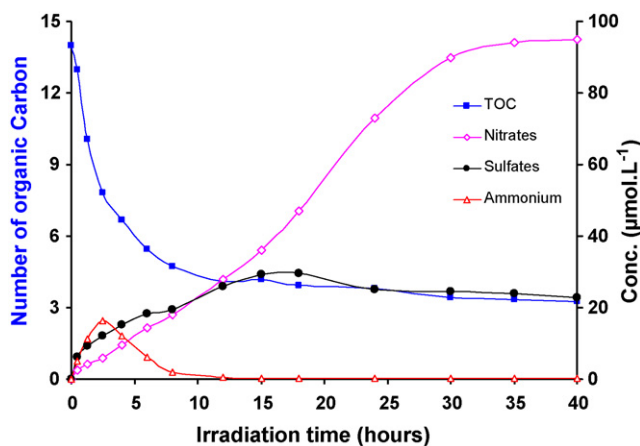
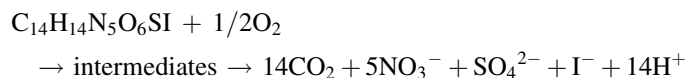


Fig. 8. Time course of TOC and inorganic ions (nitrates, sulfates and ammonium) during IOME photocatalytic degradation.

and/or NH_4^+ (regarding nitrogen content in the molecule) as well as SO_4^{2-} and I^- . The overall equation, valid after long irradiation time in the presence of excess oxygen, which describes the photocatalytic degradation of IOME is presented below:



It should be noted that nitrogen released has been measured as combination of ammonium and nitrate, but as ammonium can be oxidized to nitrate after a long irradiation time [20,21], the reaction is given here only to its most oxidized state.

Fig. 8, shows the evolution profile for TOC and inorganic ions (sulfates, nitrates and ammonium ions). The iodide (I^-) ions were not analyzed because the analytical column used was not appropriate. Regarding TOC, its kinetic evolution is represented as the number of carbon atoms per molecule of IOME. Initially, the number of C-atoms equal to 14, since there are 14 C-atoms in IOME molecule. During the first hours of irradiation, a rapid decrease in the number of C-atoms is observed, corresponding to the oxidation of the lateral chain of IOME (methoxy and methyl ester moieties), leading to the formation of products 17, 18, 11–13. Later on, the number of C-atoms decreases slowly, because of the presence of more stable intermediates, until 25 h to reach a constant number equal to 3. This finding indicates the formation of cyanuric acid as the ultimate organic product of the degradation, which is very stable towards oxidative attacks.

Regarding the inorganic ions, ammonium ions is quickly released and reaches about 16% of the stoichiometric nitrogen content after 3 h irradiation, whereas at this time approximately 5% of the total nitrogen is found as NO_3^- . Since the sum of both ions gives about 21% of the stoichiometric nitrogen, one can suggest that at this stage, 1/5 of the nitrogen atoms of IOME were transformed into NH_4^+ which is subsequently oxidized to nitrate ions. After 3 h of irradiation, ammonium concentration decrease and disappear from solution in around 4 h, whereas nitrate concentration increases slowly to reaches a plateau, corresponding to 38% of nitrogen after 40 h. This value indicates that the two nitrogen atoms of sulfonylurea bridge were completely mineralized while the nitrogen atoms of triazine ring were not touched. These results confirm the findings obtained by TOC measurements, which showed the formation of cyanuric acid as the final product of the degradation process. On the other hand, nitrates and ammonium evolution profiles indicate that one of the two N atoms of Sus bridge transforms into ammonium (first 3 h of irradiation) which is subsequently oxidized to nitrates whereas the second N atom is, later on, transformed into nitrate without passing by ammonium. Based on these results, we can suggest that N atom bound to S is released in solution as NH_4^+ whereas the N-atom substituted with the triazine ring is oxidized to $-\text{NO}_2$ and further released as NO_3^- [11]. Concerning sulfate ions, only 60% of the amount expected is obtained, assuming a total mineralization of the bridge. This could be explained by a partial irreversible adsorption of sulfates onto the TiO_2 surface

as has already been reported and/or by the formation of sulfur dioxide [22,23].

4. Conclusions

A detailed study on the photocatalytic degradation of IOME was presented, from the kinetic process to the identification of byproducts and the investigation of reactional mechanisms.

On kinetic study, degradation rate of IOME followed a pseudo-first order kinetic, suggesting an associative adsorption of the molecule on the TiO_2 surface. In addition, the degradation rate was proved to be strongly affected by the TiO_2 amount and the light flux.

On analytical study, the application of combined HPLC–MS and HPLC–NMR was demonstrated to be a very powerful approach for the identification of byproducts of the degradation. More than 20 intermediates were unambiguously identified. Moreover, the regioselectivity of the attacks of OH radicals on the aromatic ring was showed to be dependent on the electronic density of the carbon sites.

On other hand, careful monitoring of the formation of intermediates, carboxylic acids and end products permitted to obtain the detailed reaction mechanisms.

The main steps involve: hydroxylation of the benzene ring following by the ring opening leading to the formation of several short carboxylic acids, *O*-demethylation of the methoxy and methyl ester moieties, substitution of iodide atom by a hydroxyl group, oxidation of methyl and amino groups and cleavages of the sulfonylurea bridge leading to cyanuric acid which cannot undergo further attacks. Complete mineralization was therefore not achieved as has been already observed in previous studies. However, cyanuric acid is known to be innocuous, nontoxic and easily biodegradable, therefore its formation does not represent a significant danger to the environment.

References

- [1] M. Brigante, C. Emmelin, L. Previtera, R. Baudot, J.M. Chovelon, J. Agric. Food Chem. 53 (2005) 5347–5352.
- [2] J. Rouchard, C. Moulard, H. Eelen, R. Bulcke, Toxicol. Environ. Chem. 85 (2003) 103–120.
- [3] N. Serpone, E. Pellizzetti, Fundamentals and Applications, Wiley, New York, 1989, p. 650.
- [4] M. Schiavello (Ed.), Photocatalysis and Environment: Trends and Applications, NATO ASI Series C, vol. 238, Kluwer Academic Publishers, London, 1987.
- [5] D.F. Ollis, H. Al-Ekabi (Eds.), Photocatalytic Purification and Treatment of Water and Air, Elsevier, Amsterdam, 1993.
- [6] J.M. Herrmann, Catal. Today 53 (1999) 115–129.
- [7] D.M. Blake, Bibliography of Work on the Photocatalytic Removal of Hazardous Compounds from Water and Air, NREL/TP- 430-22197, National Renewable Energy, Laboratory Golden Co., 1997/1999.
- [8] E. Vulliet, C. Emmelin, J.M. Chovelon, C. Guillard, J.M. Herrmann, Appl. Catal. B: Environ. 38 (2002) 127–137.
- [9] E. Vulliet, J.M. Chovelon, C. Guillard, J.M. Herrmann, J. Photochem. Photobiol. A: Chem. 159 (2003) 71–79.
- [10] F. Fresno, C. Guillard, J. Corronado, J.M. Chovelon, D. Tudela, J. Soria, J.M. Herrmann, J. Photochem. Photobiol. A: Chem. 173 (2005) 71–79.

- [11] V. Maurino, C. Minero, E. Pellizetti, M. Vincenti, *Colloids Surf. A: Physicochem. Eng. Aspects* 151 (1999) 329–338.
- [12] S. Rafqah, P. Wong-Wah-Chung, A. Aamili, M. Sarakha, *J. Mol. Catal. A: Chem.* 237 (2005) 50–59.
- [13] M. Sleiman, C. Ferronato, B. Fenet, R. Badot, F. Jaber, J.M. Chovelon, *Anal. Chem.* 78 (2006) 2957–2966.
- [14] S. Smallcombe, S. Patt, P. Keifer, *J. Magn. Reson. A* 117 (1995) 295–303.
- [15] I. Bouzaida, C. Ferronato, J.M. Chovelon, M.E. Rammah, J.M. Herrmann, *J. Photochem. Photobiol. A: Chem.* 168 (2004) 23–30.
- [16] B. Krautler, A.J. Bard, *J. Am. Chem. Soc.* 10 (1978) 2239.
- [17] T. Tetzlaff, W. Jenks, *Org. Lett.* 1 (1999) 463–465.
- [18] C. Maillard-Dupuy, C. Guillard, P. Pichat, *New J. Chem.* 18 (1994) 941–948.
- [19] M. Karkmaz, E. Puzenat, C. Guillard, J.M. Herrmann, *Appl. Catal. B: Environ.* 51 (2004) 183–194.
- [20] E. Pramauro, M. Vincenti, *Environ. Sci. Technol.* 24 (1990) 1559–1565.
- [21] E. Pramauro, M. Vincenti, V. Augugliaro, L. Palmisano, *Environ. Sci. Technol.* 27 (1993) 1790–1795.
- [22] J.M. Herrmann, C. Guillard, M. Arguello, A. Aguera, A. Tejedor, L. Piedra, A. Fernandez-Alba, *Catal. Today* 54 (1999) 353–367.
- [23] V. Berzova, M. Jankovikova, M. Soldan, A. Blazkova, M. Rehakova, I. Surina, M. Ceppan, B. Halvinova, *J. Photochem. Photobiol. A: Chem.* 83 (1994) 69–75.